Dextrin Nanocomposites as Matrices for Solid Dosage Forms

Justin Phillips[1], Jaco-Louis Venter[1], Maria Atanasova[1], James Wesley-Smith[2], Hester Oosthuizen[1], M. Naushad Emmambux[3], Elizabeth L. Du Toit*and Walter W. Focke[1]

[1]Department of Chemical Engineering, University of Pretoria, Pretoria 0028, South Africa
[2]Sefako Makgatho Health Sciences University, Ga-Rankuwa 0208, South Africa

[3]Department of Consumer and Food Sciences, University of Pretoria, Pretoria 0028, South Africa

*Corresponding Author: Elizabeth L. Du Toit −Department of Chemical Engineering, University of Pretoria, Pretoria 0028, South Africa; orcid.org/0000-0001-5579-1231; Email: elizbe.dutoit@up.ac.za

Abstract

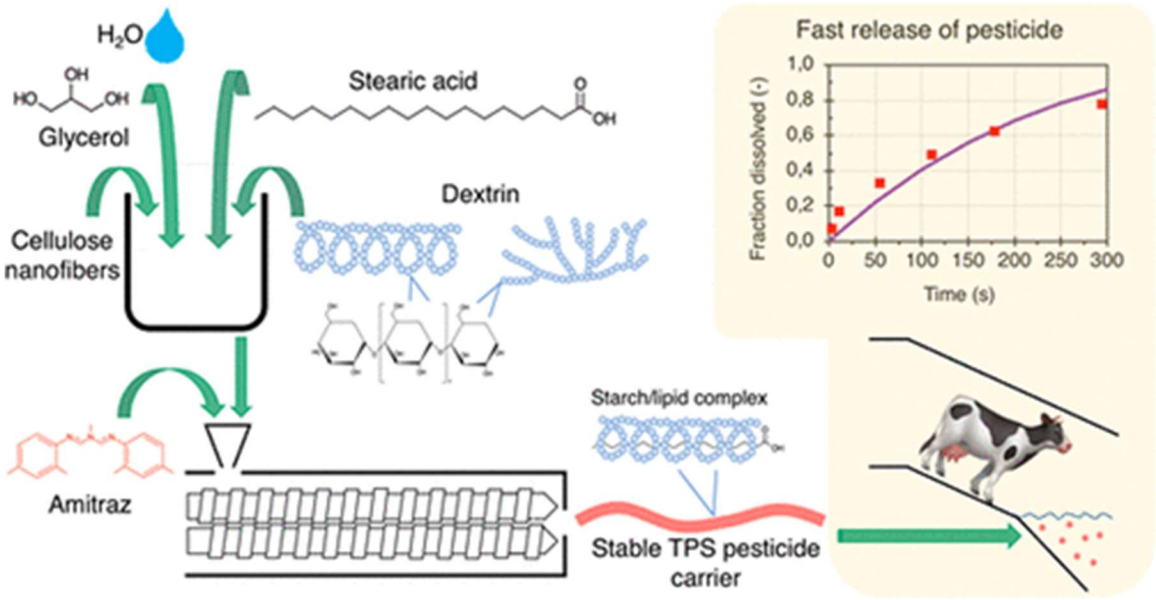

Safe application of water-insoluble acaricides requires fast release from solid dosage systems into aquatic environments. Dextrin is a water-soluble form of partially hydrolyzed starch, which may be used as matrix material for these systems if retrogradation can be inhibited by the inclusion of nanofillers. Several glycerol-plasticized thermoplastic dextrin-based nanocomposites were prepared with a twin-screw extrusion-compounding process. The nanofillers included a layered double hydroxide (LDH), cellulose nanofibers (CNF), and stearic acid. The time-dependent retrogradation of the compounds was monitored by X-ray diffraction (XRD) and dynamic mechanical thermal analysis (DMA). XRD showed that composite samples that included stearic acid in the formulation led to the formation of an amylose-lipid complex and a stable crystallinity during aging. The most promising nanocomposite included both stearic acid and CNF. It was selected as the carrier material for the water-insoluble acaricide Amitraz. Fast release rates were observed for composites containing 5, 10, and 20% (w/w) of the pesticide. A significant reduction in the particle size

of the released Amitraz powder was observed, which is ascribed to the high-temperature compounding procedure.

KEYWORDS: dextrin; cellulose nanofibers; layered double hydroxide; solid dosage form; acaricide; themoplastic starch

Introduction

Controlled-release formulations for pesticide applications act as depot systems that continuously release active ingredients into the environment over a specified period, usually from months to years.[1,2]However, some applications require quicker dissolving drug delivery.[3,4)]This is specifically true when insoluble pesticides, like acaricides, must be released into aquatic environments for cattle treatment. Suitable physical forms include tablets, granules, and fibers that either disintegrate or dissolve to release a water-insoluble active ingredient as fine particles. Compared to wettable powders, they offer good flowability and a reduced risk of dust inhalation.[5] These types of dosage forms can be fabricated using a variety of processes[5] including lyophilization, spray drying, solvent casting, hot melt extrusion,[6,2] compression molding, wet granulation, compaction, and electrospinning.[4,7]

Starch is a carbohydrate biopolymer that is abundant, inexpensive, and fully biodegradable. It can be converted into a thermoplastic starch (TPS) by applying shear and heat in the presence of water and plasticizers such as glycerol. This is typically done via an extrusion compounding operation[8] during which the starch granules undergo an order–disorder phase transition called gelatinization.[9] The transformation involves diffusion-driven penetration of the water and the plasticizer resulting in the hydration and swelling of the starch particles. The consequence is a progressive loss of crystallinity and ultimately complete amorphization of the starch.

Unfortunately, the hydrophilic nature of starch means that it has some undesirable properties that limits its use in many applications.[10] For example, following melt processing, thermoplastic starch (TPS) suffers from warpage, shrinkage, and embrittlement.[11,12] This is due to retrogradation, the slow recrystallization of the amylopectin fraction, and the fast recrystallization of the amylose part.[13] Fortunately, modification of thermoplastic starch with special plasticizers and other additives tends to ameliorate these weaknesses. Suitable plasticizers such as isosorbide,[14,15] fatty acids,[10,16,11] nanoclays,[17] and cellulose nanofibers[18,13,19] have shown promise to reduce the rate of retrogradation of TPS. Additionally, the nanofiller additives are also effective as reinforcements.

Dextrin is a water-soluble form of partially hydrolyzed starch. It is a very low molar mass material obtained by acid-catalyzed or enzymatic hydrolysis of starch. The extent of hydrolysis of the starch is quantified by the dextrose equivalent (DE), a quantifier that is inversely related to the degree of polymerization.[20] Because of the lower molar mass, it is particularly easy to convert dextrin into a thermoplastic material by using melt processing.[21] The aim of the present study was to investigate the effect of the inclusion of different combinations of stearic acid, cellulose nano fibers (CNF) and layered double hydroxide clay (LDH) on the processability, morphology, mechanical properties, and aging behavior of a

dextrin-based water-soluble thermoplastic starch. A simple melt-extrusion procedure was considered to produce the composite materials. The targeted application was to produce a stable TPS matrix that could serve as solid dosage system for the water-insoluble acaricide, Amitraz. Subsequently, Amitraz was incorporated into the best-performing composite material and the aquatic release behavior was characterized.

Materials and Methods

Materials

Tongaat Hulett supplied Stydex White Dextrin 072012. The degree of polymerization of this samples was estimated as DP = 53 ± 5. Details are presented in the Supporting Information. Spherical 4070AH 40 μm glass beads were purchased from Blastrite. Greenfield Additives provided a sample of grade B44 calcium–aluminum layered double hydroxide (LDH). This material was previously identified as hydrocalumite, i.e., a calcium hemicarboaluminate.[22] In this clay, half the interlayer carbonate ions are substituted by hydroxyl ions. Sappi donated Valida-Visco-L, a fibrillated nanocellulose fiber (CNF) suspension containing 13.4 wt % solids. Glycerol of purity >99.5% was purchased from Associated Chemical Enterprise. Pristerine 4989 technical grade stearic acid was obtained from Protea Chemicals. Technical grade 98.5% Amitraz was donated by Bayer. Sigma-Aldrich supplied reagent-grade iodine, anhydrous potassium iodide, and sodium nitrate.

Sample Storage and Conditioning

All starting materials, compounded granules, and pressed sheets were stored at room temperature in a large plastic container. The inside atmosphere was controlled to a relative humidity of 75% via the presence of a supersaturated sodium chloride solution.[23]

Methods

Milling

A portion of the LDH was milled on a Netsch LME1 laboratory-scale horizontal stirred bead mill operated at 2000 rpm. Zircon beads, with a diameter of 250 μm, functioned as the milling medium. A slurry, made up by suspending 800 g of LDH in 8.0 L of distilled water, was continuously pumped through the mill. The recirculating flow protocol was maintained for a period of 3 h. The resulting slurry was used directly in the preparation of the corresponding dextrin nanocomposite.

Dextrin Nanocomposites

All the dextrin nanocomposite compounds were formulated to contain 60 wt % dextrin, 18 wt % glycerol, 18 wt % deionized water, and a total of 4 wt % additives as listed in Table 1. The base thermoplastic compound (sample S7), used as carrier for the Amitraz acaricide, contained 3 wt % stearic acid and 1 wt % CNF (S7). Compounds containing 5, 10, and 20 wt % Amitraz were prepared using this material as carrier. It proved impossible to process compounds that contained more than 1 wt % of the nanocellulose fibers. Therefore, the

spherical glass spheres were included as inactive filler to control the additive content at 4 wt % for all compounds. The assumption was that the small amount of a spherical filler has a negligible effect on mechanical properties. Furthermore, this approach allowed property comparisons to be made with all compounds having a fixed dextrin, water, and plasticizer content. This meant that the reference dextrin TPS composition contained 4 wt % glass spheres.

Table 1. Additive Combinations Used to Prepare the Dextrin Nanocomposites[a]

#	TPS compound	GB	LDH	CNF	SA
S0	no additives				
S1	glass beads (GB)	4.0			
S2	LDH (unmilled)		4.0		
S3	cellulose nanofiber/GB 1:3	3.0		1.0	
S4	stearic acid (SA)				4.0
S5	milled LDH		4.0		
S6	LDH/stearic acid 1:1		2.0		2.0
S7	stearic acid/CNF 3:1			1.0	3.0
S8	LDH/CNF 3:1		3.0	1.0	
S9	ternary: LDH:SA:CNF 1.5:1.5:1		1.5	1.0	1.5

[a]The numbers represent the concentrations in units of wt %.

Extrusion Compounding

Blends, totaling 400 g, were prepared in 5 L HDPE containers. The required quantities of each compound were weighed out and mixed thoroughly with the help of a plastic paddle. The blends were extrusion-compounded on a ThermoFischer TSE 24 corotating twin-screw compounder (24 mm φ, 30 L/D). The compounder die had a single exit hole with a diameter of 5.5 mm. The screw speed ranged from 50 to 80 rpm as it was found necessary to adjust it for each individual formulation. The temperature profile, from hopper to die, was controlled to 60/80/100/110/110/110/110 °C for the neat dextrin TPS nanocomposites. These process conditions yielded exiting polymer strands with acceptable melt strengths that allowed them to be pulled. The control temperatures had to be lowered when compounding the Amitraz-filled compounds because of the reduction in the apparent melt viscosity and loss of melt strength due to due to the dissolution of Amitraz in the melt. They were set at 60/80/90/100/100/100/100 °C for the 5 and 10 wt % Amitraz compounds and to 60/80/90/95/95/95/95 °C for the compound containing 20 wt % of the acaricide.
All extruded strands were stored overnight at a temperature of −10 °C before they were granulated into pellets approximately 4–6 mm in length.

Sheet Pressing

The granulated samples were recompounded with the die attachment removed from to the compounder. Portions of the hot exiting melt were swiftly collected and pressed between two metal plates covered with polyester films. This was done to avoid material sticking to

the metal surfaces. A metal frame separator was used to control the sheet thickness to ca. 1.6 mm.

Characterization

Moisture Content

The moisture content of the conditioned compounds was determined with an Ohaus MB35 moisture analyzer. The analyzer was used in the "auto" setting with the control temperature set at 120 °C. The average of at least duplicate measurements is reported.

Particle Size Distribution (PSD)

The particle size distributions of the raw materials and the dextrin based TPS compositions were determined on a Malvern Mastersizer 3000 coupled with a Malvern LV Hydro. The materials were dispersed in deionized water and the reported results represent the average of five measurements.

Scanning Electron Microscopy (SEM)

Prior to microscopy, the granules were submerged in liquid nitrogen before fracturing into small fragments to expose their interior structure. The samples were sputter coated with chromium and viewed using a Zeiss Supra 55 FEGSEM at 5 kV.

High-Pressure Differential Scanning Calorimetry (HPDSC)

Differential scanning calorimetry was conducted on a HP SC827e Mettler Toledo instrument under a nitrogenous pressurized atmosphere at 4 MPa. An empty aluminum pan (100 µL) was used as reference. An ∼40 mg sample was sealed into a perforated aluminum pan. Samples were heated from 20 to 200 °C at a heating rate of 10 K min^{-1}. The instrument was calibrated using an indium standard.

Dynamic Mechanical Thermal Analysis (DMA)

Rectangular strips (35 mm × 10 mm) were cut from the sample sheets. The sheet thickness was measured with a Mitutoyo RHS 769 µm. The viscoelastic behavior was studied with a PerkinElmer Dynamic Mechanical Analyzer 8000 in the single cantilever bending mode. The strain amplitude was set at 20 µm and the applied frequency was 1 Hz. The temperature was scanned from −90 to 40 °C at a scanning rate of 1 K min^{-1}. It proved difficult to obtain reliable DMA results as the temperature approached 20 °C. The tan δ values, in particular, showed considerable scatter, often leading to premature termination of the scans. Unfortunately, the DMA results indicated that the glass transitions of all the nanocomposite samples was located in the vicinity of this temperature. It was necessary to estimate the probable T_g values using the parabolic curve fitting technique illustrated in the Supporting Information.

X-ray Diffraction (XRD)

XRD measurements were performed on a Bruker D8Advance diffractometer set to 2.2 kW Cu Kα radiation with a wavelength of 1.54060 nm and LynxEye detector with 3.7° active area. Sheet samples of the composite materials were cut into 22 mm φ discs. The samples were scanned in reflection mode from 2 to 70° 2θ at a rate of 0.02° s^{-1} at generator settings of 40 kV and 40 mA. XRD scans were performed on the first day after extrusion (day 1) and then on intermittent days up to a total aging time of 98 days. In between measurements, the samples were stored at ambient conditions at 75% relative humidity. Samples of the pure materials were subjected to the same analysis protocol in order to obtain characteristic diffractograms used to identify reflections associated with each of the components. The ICDD database PDF-2 2015 was used for phase identification and the PDF card reference for each of the starting materials is cited in the discussion part of the text.

The degree of crystallinity was calculated following a methodology similar to the one described by Frost et al.[24] First, Savitzky-Golay smoothing was applied to the original data. After baseline subtraction, the crystallinity was estimated by the ratio of the sum of all the areas under each reflection peak to the total area under the diffractogram curve over the 2θ range 5–45°. The procedure is illustrated in Figure S1 Supporting Information.

Dissolution

The granulated samples were sieved and the granules in the size range of 4.0–4.75 mm were collected. A 0.1 M iodine solution was prepared by dissolving 20 g of KI and 6.4 g of I_2 in 500 mL of deionized water.[25] It was used as indicator for the determination of the temporal variation of the starch concentration in each dissolution experiment. Spectra were recorded on a PG Instruments T60 UV–visible Spectrophotometer. The dissolution of the water-soluble dextrin was used as a proxy for the release of the Amitraz. The absorbance measured at a wavelength of 580 nm and Beer–Lambert's Law was used to generate the calibration curve based on a range of dextrin solutions.[25]

Duplicate dissolution experiments were conducted for each sample in a laboratory temperature-controlled to 20 ± 1 °C. In each case, approximately one gram of the sieved granules was added to a 1.0 L Erlenmeyer flask containing 500 mL deionized water and 2.00 mL of the 0.1 M iodine solution. The flask contents were vigorously agitated using a magnetic stirrer operating at a speed set to 200 rpm. At intermittent times, 5.0 mL sample liquid was removed from the flask and rapidly filtered. The liquid filtrate was analyzed in a polystyrene cuvette in the spectrometer and the dextrin concentration was calculated from the measured absorbance. The dissolution data were regressed using the Hixson–Crowell model.[26,27]

$$1 - [M(t)/M_0]^{1/3} = t/\tau \quad (1)$$

where $M(t)$ is the mass remaining at time t; M_0 is the initial mass, and τ is the dissolution time of the granules. Strictly speaking, the Hixson–Crowell model is applicable for isotropic dissolution, under sink conditions, of spherical particles and cylinders of equal length and diameter.[27] This means that the model assumes that the solubility limit far exceeds the final concentration obtained on complete dissolution of the granules. The characteristic time constant depends on the granule geometry, the fluid flow conditions, as well as physical

properties such as density, the diffusion coefficient and the solubility of the material in water. The Hixson–Crowell dissolution time (τ) is independent of the granule size at a fixed temperature when geometric similarity (proportional granule dimensions) and dynamic similarity both hold. The latter conditions require equivalent Reynolds Numbers characterizing the flow field.

Results

Layered Double Hydroxide (LDH) Particle Size

The D5, D10, and D90 particle sizes of the LDH were found to be 4.98, 10.9, and 19.9 µm, respectively. These values decreased to 3.12, 8.68, and 16.9 following the bead milling process. A more complete characterization of the LDH was presented elsewhere.[22]

Compound Morphology

An interesting observation made during the compounding was the flow stability imparted to the TPS when CNF was present as an additive. Its presence significantly improved the melt strength of the exiting strand. It also yielded strands with a smoother surface.

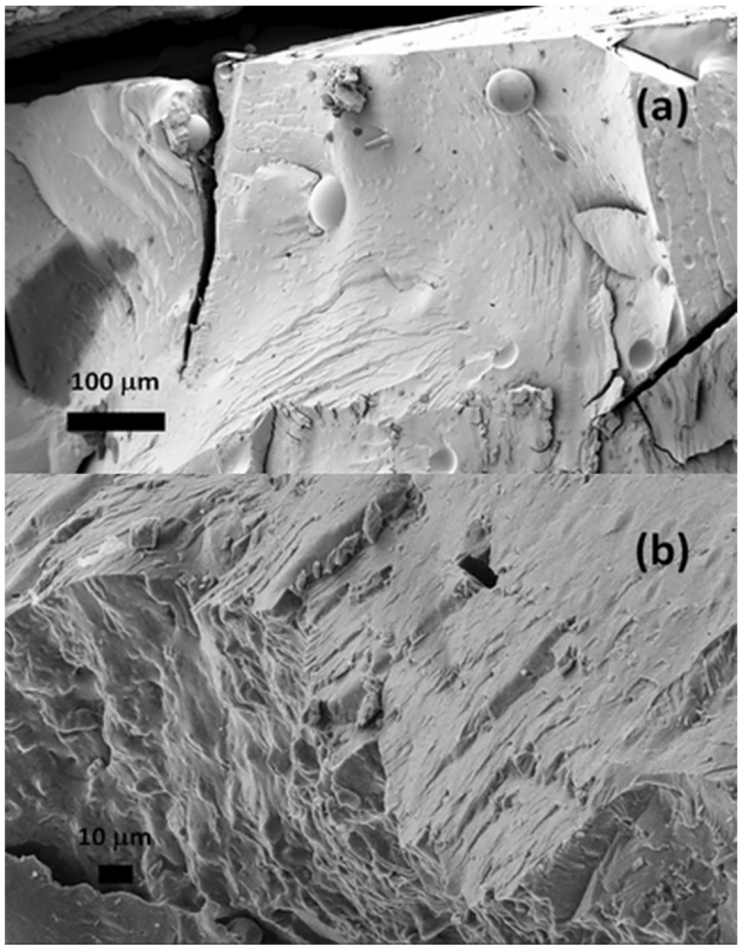

Figure 1. SEM micrographs of (a) Sample S1 (glass-containing dextrin-based TPS) and (b) Sample S7 (compound containing 3.00 wt % stearic acid and 1.00 wt % cellulose nanofibers).

Figure 1 shows scanning electron micrographs of the surfaces of freeze-fractured samples S1 and S7. The spherical glass beads are evident in the image of sample S1. At the resolution shown, the materials appear monolithic and the texture of the surfaces are consistent with the expectations for the fracture of brittle glassy amorphous materials.

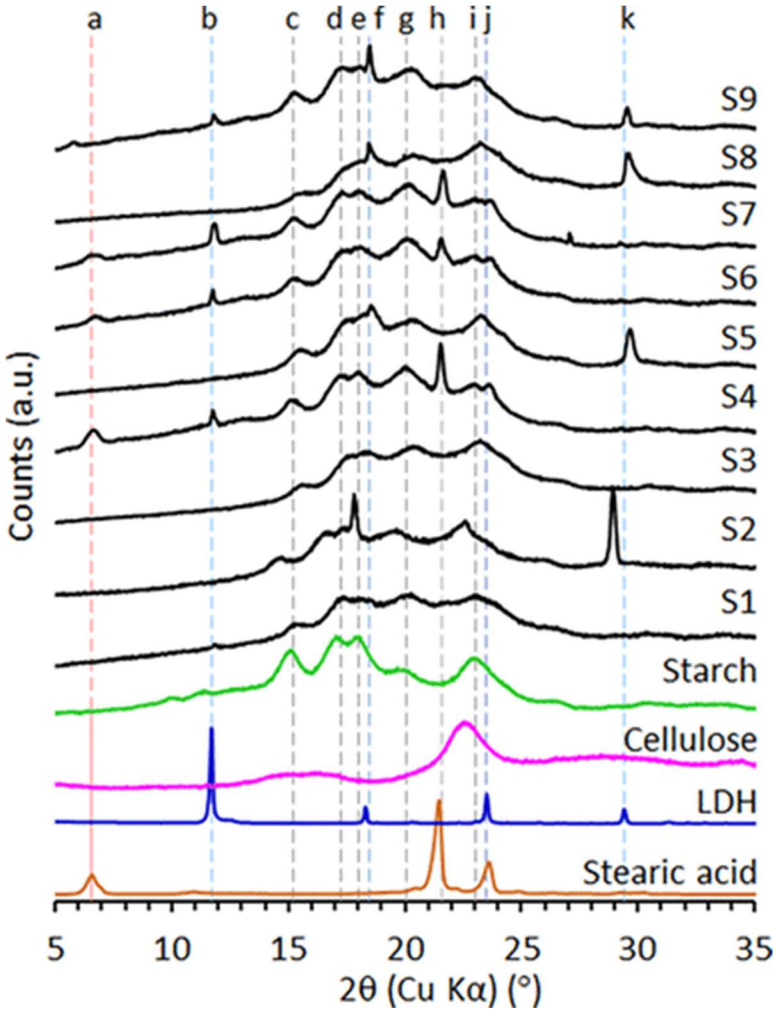

Figure 2. XRD diffractograms of the nanocomposites aged for 98 days compared to those of the starting materials. Details on prominent reflections, labeled a–k, are given in Table 2

Figure 2 compares the XRD diffractograms of the aged nanocomposites to those of the starting materials. The main reflections are listed in Table 2. The XRD diffractogram of the native dextrin, identified as α-amylose $(C_6H_8O_4)_n$ (PDF 00–043–1858), features strong reflection peaks at 2θ = 15.1° (*d* = 0.586 nm), a doublet at 17.2° (*d* = 0.516 nm)/17.9° (*d* = 0.493 nm), and another strong reflection at 23.0° (*d* = 0.387 nm) typical for a type A crystallinity.[8] In raw starch this type of crystallinity is attributed to chains arranged in a double helical structure.[8,28] Just as for conventional thermoplastic starches, the diffraction pattern of the dextrin-based TPS featured an extensive amorphous scanning halo with weaker diffraction peaks. This is typical for semicrystalline polymers with a low crystallinity.[24] Usually the TPS gelatinization process destroys the original crystalline structure and induces a different, processing-induced crystallinity. Depending on variables such as the type and amount of plasticizer and the intensity of the applied shear, three

types of induced crystalline structures, i.e., V_H, V_A, and E_H type, are obtained. [8,28] The V type crystallinity arises from the packing of single helix chains, mostly amylose, with ligands such as stearic acid. These are known as amylose lipid complexes. The latter occur in anhydrous (V_A) or hydrated forms (V_H) with interhelical water molecules present in the latter.[29] The present dextrin-based TPS samples featured a combination type V_A type crystallinity superimposed on the original A type polymorphism. This means that the neat TPS, as well as most of the nanocomposites, either recovered or retained the type A crystallinity present in the native dextrin. This behavior can be attributed to the fact that the dextrin starch base comprises primarily rather short chains as this favors type A crystallinity.[30] In addition, the associated much lower melt viscosity may facilitate rapid reorganization after melting in the compounding process. The results suggest that there were essentially linear dextrin chains that can form V type complexes with ligands as well as self-association to form double helical type A structures.

Table 2. Crystallographic Parameters Associated with the Most Prominent Reflections in the Diffractograms of the TPS Nanocomposites

#	2θ (deg)	*d* (nm)	assignment
a	6.7	1.31 ± 0.02	stearic acid
	11.1	0.79 ± 0.02	stearic acid
b	11.7	0.76 ± 0.00	LDH
c	15.1	0.58 ± 0.01	starch
	15.6	0.57 ± 0.01	stearic acid
	15.7	0.56 ± 0.02	CNF
d	17.2	0.52 ± 0.01	Starch
e	17.9	0.49 ± 0.01	Starch
f	18.4	0.481 ± 0.003	LDH
g	20.1	0.442 ± 0.005	Starch
h	21.5	0.414 ± 0.006	Stearic acid or
	21.6	0.412 ± 0.008	SA-starch V-complex
i	22.9	0.39 ± 0.01	CNF
	23.0	0.387 ± 0.003	Starch
j	23.5	0.378 ± 0.010	LDH
	23.6	0.377 ± 0.004	Stearic acid
k	29.4	0.302 ± 0.003	LDH

The strong reflection at 22.9° (*d* = 0.386 nm) in the diffractogram for the nanocellulose fibers, identified as Cellulose Iβ (PDF 00-056-1718), is typical of the cellulose I pattern.[31] There is also an indication of this reflection in the XRD pattern of the TPS cellulose nanocomposite (sample S3) but not in any of the other composites that contain CNF.

The diffractogram for the LDH, identified as calcium aluminum hydroxide carbonate hydrate (PDF 01-087-0493), features prominent reflections at 11.7 (*d* = 0.755 nm), 18.3 (*d* = 0.48 nm), 23.5 (*d* = 0.38 nm), and 29.54° (*d* = 0.30 nm). The diffractogram for the LDH-based dextrin TPS nanocomposite (sample S2) shown in Figure 2 shows only two of these reflections as very strong and sharp peaks albeit at slightly higher *d*-spacing values (0.50 and 0.31 nm, respectively). Figure 3a shows the time evolution of the XRD pattern for this nanocomposite. The main LDH reflection is clearly visible on day 1 and at diminished

intensity on day 3. However, it is absent in the diffractograms recorded on later days. Similar observations apply to the TPS nanocomposites obtained with either the milled LDH (sample S5) or LDH+CNF combination (sample S8). However, the main LDH reflection at 11.7° (*d* = 0.77 nm) is retained indefinitely in the nanocomposites based on the stearic acid plus LDH combination (sample S6) as well as in the ternary additive mixture (sample S9). The implication is that, in the absence of stearic acid, either the LDH in the nanocomposites delaminates on aging or it is degraded into compounds that do not feature the reflections associated with the hydrocalumite.

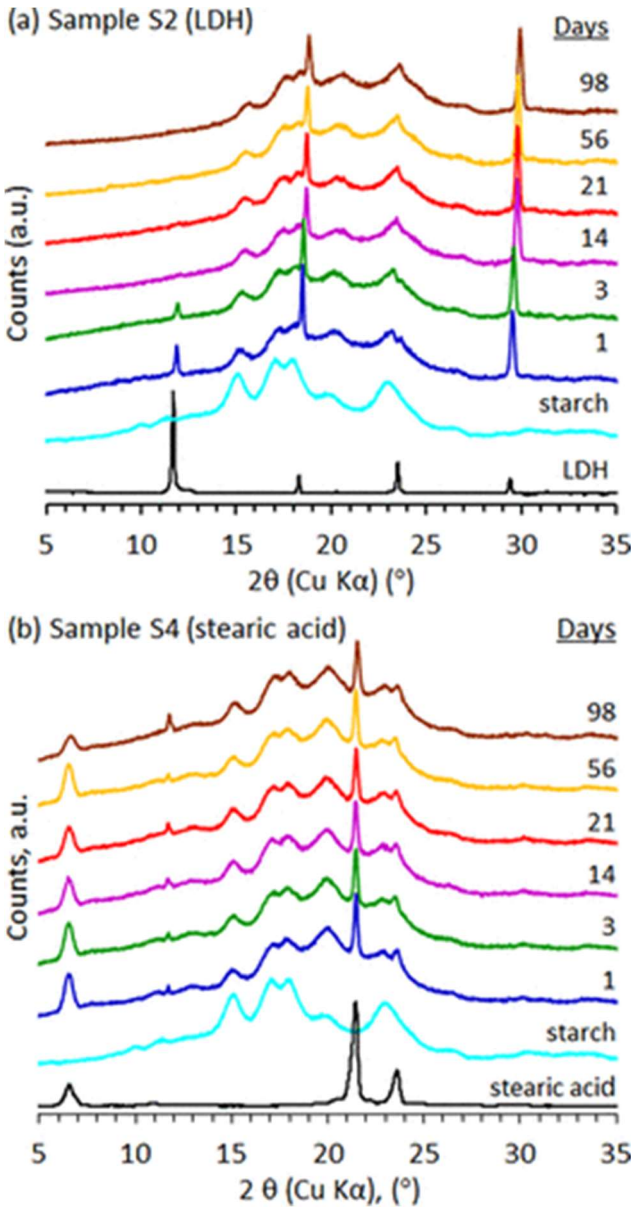

Figure 3. Time evolution of the XRD diffractograms for (a) the LDH-based nanocomposite (sample S2), and (b) for the stearic acid–based compound (sample S4).

The three most prominent reflections in the XRD pattern for stearic acid (PDF 00–038–1923) are located at 6.7° (*d* = 1.32 nm), 11.1° (*d* = 0.79 nm), and 15.6° (*d* = 0.57 nm). Figures 2 and 3b show that the stearic acid-based TPS nanocomposite (sample S4) has particularly interesting diffractograms. The patterns recorded at day 1 and at all subsequent times are

virtually identical. They show two important reflections at low angles that appear to correspond to the first two for the neat stearic acid. However, both are shifted to lower angles. The first shows a significantly broadened peak at 6.7° (*d* = 1.32 nm), whereas the second appears sharper and is located at 11.7° (*d* = 0.75 nm). However, the most prominent feature of this diffractogram is the strong and sharp reflection located at 21.6° (*d* = 0.41 nm). It is attributed to the V complex formed with the stearic acid. The arrested retrogradation of sample S4 might be due to the creation of this more stable starch-lipid complex.[13] This complex is observed in all the diffractograms of the nanocomposites that contain stearic acid (samples S4, S6, and S7) but, oddly, not in that of the ternary nanocomposite (sample S9).

Table 3 lists the calculated degrees of crystallinity for each nanocomposite compound as a function of aging time. The last column shows the ratio of crystallinity estimated on day 98 to that measured from the diffractogram obtained on day 1. In all cases, crystallinity increased with aging time with the intensity of particular reflectances changing substantially in some samples. Table 3 shows that the crystallinity of the neat dextrin TPS (sample S1) increased by about 36% on aging. The change was less for the compounds containing additives and it was negligible for the stearic acid-based nanocomposite (sample S4).

Table 3. Estimated Crystallinity of the Dextrin Nanocomposites

	relative crystallinity (%) on day						
sample	**1**	**3**	**14**	**23**	**56**	**98**	**ratio[a]**
S1	1.13	1.18	1.58	1.49	1.57	1.50	**1.36**
S2	4.74	4.97	4.70	4.86	5.19	5.21	**1.05**
S3	3.31	3.59	3.68	3.64	3.82	3.64	**1.12**
S4	4.33	4.27	4.37	4.45	4.29	4.43	**1.01**
S5	4.84	5.12	5.12	5.37	5.35	5.42	**1.10**
S6	3.70	3.72	4.13	4.06	4.12	4.93	**1.16**
S7	4.15	4.35	4.51	4.26	4.40	4.48	**1.06**
S8	4.49	4.87	4.58	4.57	5.13	4.90	**1.07**
S9	4.08	4.33	4.76	4.49	4.79	4.56	**1.14**

[a]Crystallinity averaged over last three measurement relative to Day 1.

Table 3 indicates that all compounds were predominantly amorphous in nature with very low degrees of crystallinity. The crystallinity of the neat TPS increased from about 1.13% on day 1 to just 1.36% on day 98. The highest crystallinities were found for the two LDH-based nanocomposites. Even in this case, the change was from about 4.7% to just over 5.4%. Stearic acid and LDH, on their own, are highly crystalline compounds and the nanocellulose fiber was partially crystalline. It could therefore well be that the difference in the crystallinity values of the samples simply reflects the contribution of the crystalline additives that they contain. To test this hypothesis, an attempt was made to predict the crystallinity based on a linear blending rule:

$$X = X_{\mathrm{TPS}} + C_{\mathrm{CNF}} w_{\mathrm{CNF}} + C_{\mathrm{SA}} w_{\mathrm{SA}} + C_{\mathrm{LDH}} w_{\mathrm{LDH}} \quad (2)$$

where X is the steady-state crystallinity (in %) of the nanocomposite after aging. This was taken as the average value for measurements made at times exceeding 21 days of aging. X_{TPS} = 1.54% is the crystallinity of the neat TPS; w_i is the mass fraction (in wt %) and C_i is an adjustable constant quantifying the contribution of additive i. A least-squares fit yielded C_{CNF} = 1.20; C_{SA} = 0.63, and C_{LDH} = 0.84. Figure 4 shows a plot of the predicted crystallinity values versus the steady-state crystallinity. This suggests that the model fits the data reasonably well except for the cellulose nanofiber composite (sample S3). The correlation coefficient is R = 0.966 with this value included. Also shown in Figure 4 is a plot of the crystallinity on day 1 against the steady-state value. These values fall on a line with a slope of unity and a correlation coefficient of R = 0.988.

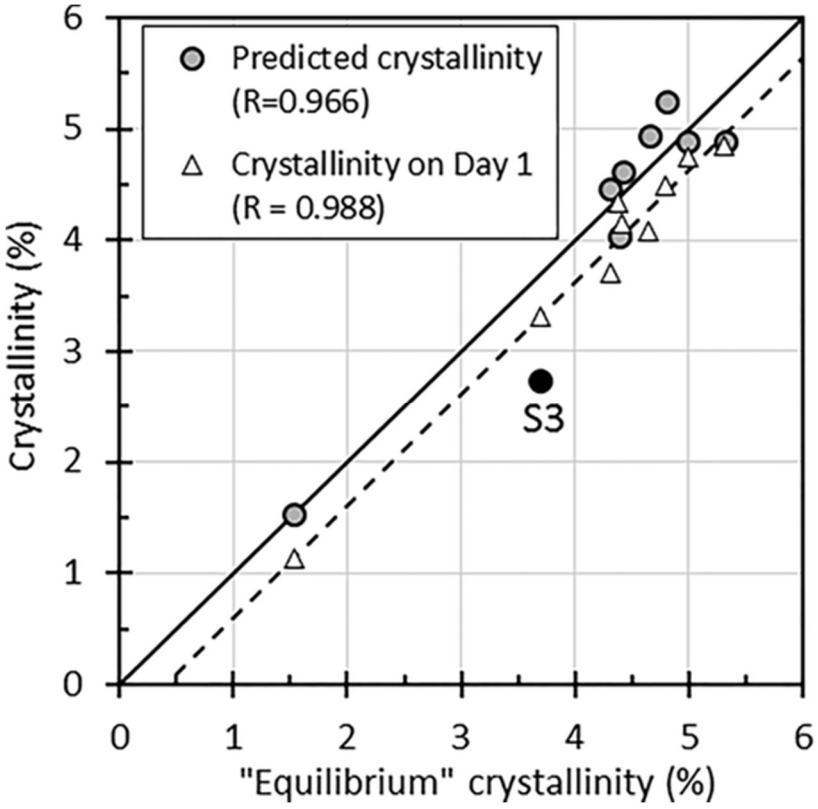

Figure 4. Correlations between the steady-state crystallinity (○); the values predicted by eq 1 (solid line), and the values measured on day 1 (Δ). The crystallinity of sample S3 appears to be an outlier (●).

If the additive is perfectly crystalline, a value of unity for the corresponding C_i implies direct additivity and the absence of an interaction with the dextrin matrix. The value C_{CNF} exceeds unity, which indicates that the presence of the cellulose nanofiber leads to a slightly larger crystallinity than expected. This could imply that the CNF acts as a weak nucleating agent for the dextrin but in order to prove this, further experimentation is required. The opposite is true for the stearic acid and the LDH. In the case of stearic acid, the formation of the SA-dextrin V complex may explain the lower-than-expected crystallinity. When this complex forms, the stearic acid molecules enter the single-chain starch helices, stabilizing that particular form. However, it means that the molecules available for crystallizing as a separate stearic acid phase is reduced. The lower-than-expected crystallinity for the LDH compound (sample S2) is consistent with the notion that it exfoliated on incorporation into the TPS.

Moisture Content

Table 4 lists the equilibrium moisture contents of the nanocomposites after extensive aging at room temperature and a relative humidity of 75%. All values were within 1.5 wt % of the expected 18.0 wt % water content of the original formulations.

Table 4. Moisture Content, Bending Modulus, Beta Transition Temperature and Glass Transition Temperature Estimates Determined for the TPS Nanocomposites

sample	moisture[a] (wt.%)	T_β (°C)	T_g (°C)	E' at 20 °C (GPa)
S1	16.9 ± 0.5	–59, −58	14	1
S2	16.3 ± 0.0	–56, −54	23	2.5
S3	15.0 ± 0.2	–55, −57	21	3.2
S4	16.7 ± 0.4	–59, −60	13	1.2
S5	18.1 ± 0.0	–56, −54	32	3.4
S6	18.6 ± 0.4	–56, −56	19	1.9
S7	17.8 ± 0.8	–58, −59	21	3.2
S8	17.8 ± 0.1	–59, −55	23	3
S9	18.4 ± 0.2	–56, −58	17	2.4

[a]Moisture content after aging at ambient temperature and 75% relative humidity.

Differential Scanning Calorimetry (DSC)

Figure 5 compares the DSC thermogram of the neat TPS to those of the nanocomposites containing stearic acid. In these samples, the stearic acid contents correspond to 0, 1.5, 2.0, 3.0, and 4.0 wt %. The stearic acid melting endotherm, peaking at ca. 57 °C, is clearly visible in samples S4 and S7, which contained 3.0 and 4.0 wt % of this additive, respectively. This endotherm is not present in the samples that contained less stearic acid. The broad endotherm located in the temperature range 120 to 140 °C is attributed to the type IIb V type amylose lipid complex,[29] which is consistent with the interpretation of the XRD data. The peak temperature associated with this endotherm decreases from 132 to 125 °C as the stearic acid content decreases from 4.0 to 1.5 wt %. The implication is that the dextrin becomes saturated, with respect to complex formation, at stearic acid concentrations between 2 and 3 wt %.

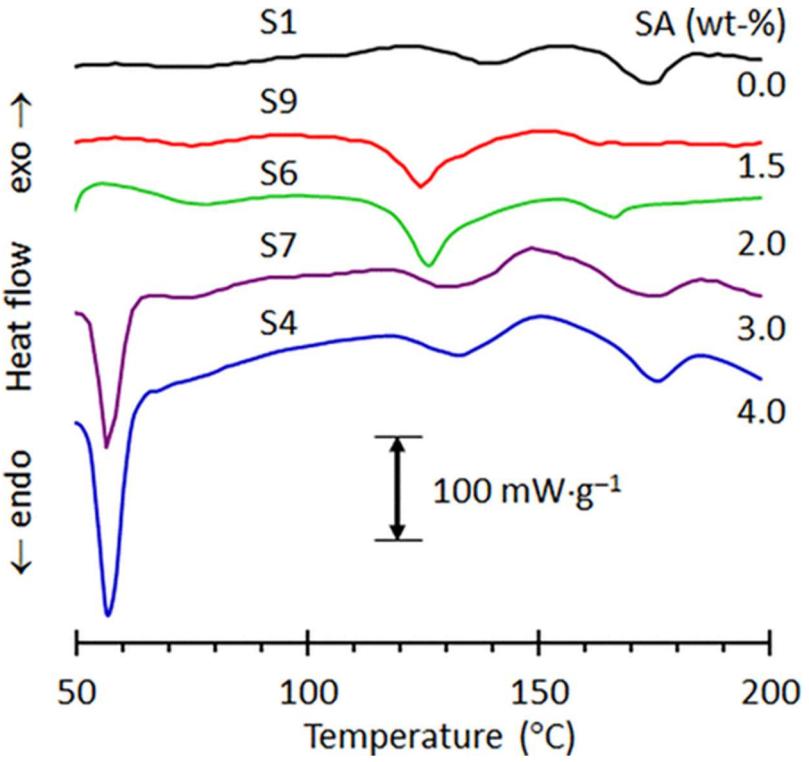

Figure 5. Differential scanning calorimetry (DSC) results for stearic acid-containing composites compared to the behavior of the neat TPS.

Dynamic Mechanical Analysis (DMA)

Figure 6 shows a typical DMA result obtained for a sheet of Sample S4 in single cantilever bending mode. Additional results are presented in Figure S2 in the Supporting Information. As illustrated in this Figure and the summarized results presented in Table 4, all compounds showed more or less similar modulus vs temperature trends. The modulus curves for the nanocomposites were displaced vertically compared to the dextrin TPS (sample S1). All the compounds exhibited a pronounced β transition at a similar temperature of ca. – 57 ± 2 °C. The glass transition of the neat dextrin TPS was ca. 14 °C. The glass transition temperatures of the nanocomposites seemed to be slightly higher by about 7 °C. Unfortunately, the severe scatter in the DMA tan δ signals, as the temperature of approached 20 °C and illustrated in Figure 6, meant that the glass transition temperatures could not be determined to high accuracy. This means that the values listed in Table 4 provide a rough guide only. It is possible that the apparent differences might be an artifact of the measurement technique.

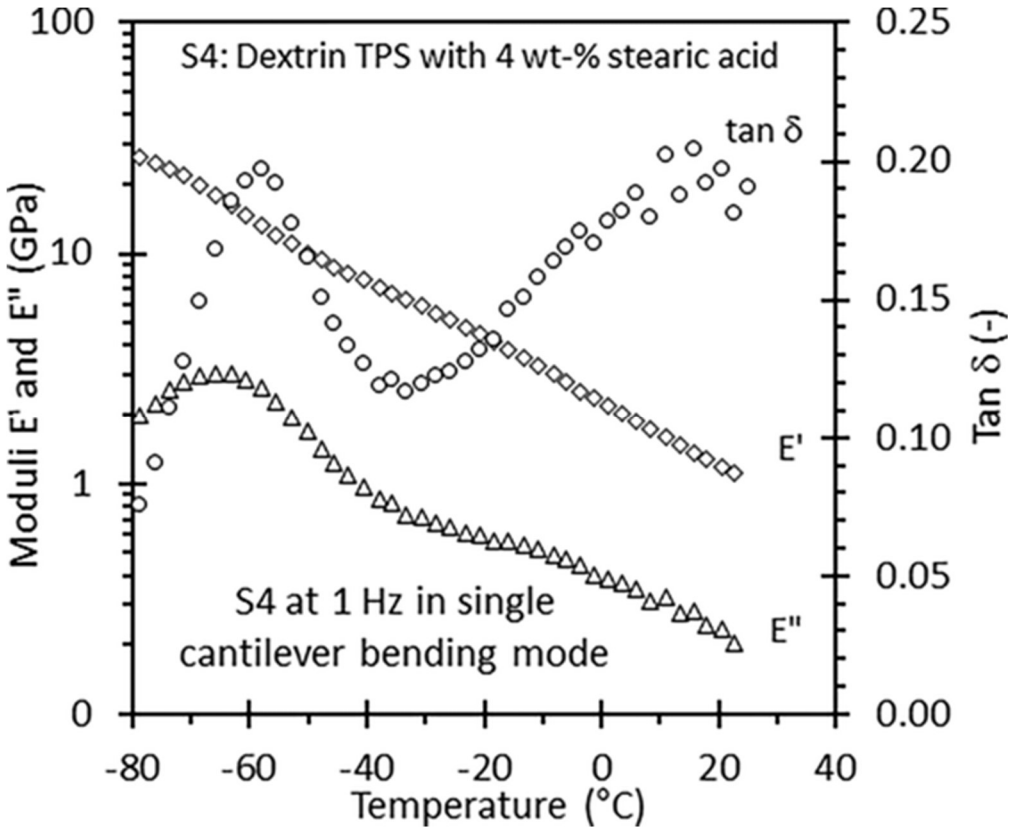

Figure 6. DMA results obtained in single cantilever bending mode at 1 Hz for nanocomposite sample S4 (dextrin nanocomposite containing 4 wt % stearic acid).

Table 4 also lists values of the bending modulus at 20 °C as determined by DMA. The results indicate that the CNF and LDH nanoparticles led to a significant increase in the bending modulus. Compounds containing them were up to three times stiffer than the glass-filled base compound. Comparing sample S5 to sample S2 shows that the milled LDH was more effective than the unmilled material as a reinforcing filler. The CNF appears to be particularly effective considering that loadings of just 1 wt % provided stiffness increases exceeding a factor of 3 (samples S3 and S7). The result for sample S4 shows that the stearic acid on its own did not impart a reinforcement effect.

Dissolution in Water

Figures 7 and 8 show plots quantifying the dissolution data for selected neat TPS compounds. Figure 7 shows actual dissolution plots for sample S7, which is based on the combination of stearic acid and CNF, sample S8 (based on LDH plus stearic acid) and for the ternary compound (sample S9), which took the longest time to dissolve. Figure 8 shows the dissolution times (τ) extracted by fits of the data using the Hixson–Crowell model expressed as a direct proportionality to the dissolution time as shown in eq 1. The error bars represent 95% confidence intervals for the dissolution times. The much longer dissolution time of the ternary nanocomposite shown in Figure 8a, compared to those of the other compounds, is statistically significant. On face value, the trends indicate that inclusion of stearic acid and CNF lead to longer dissolution times. The opposite effect is observed on adding LDH, except when stearic acid is also present. The reasons for these observations are not clear.

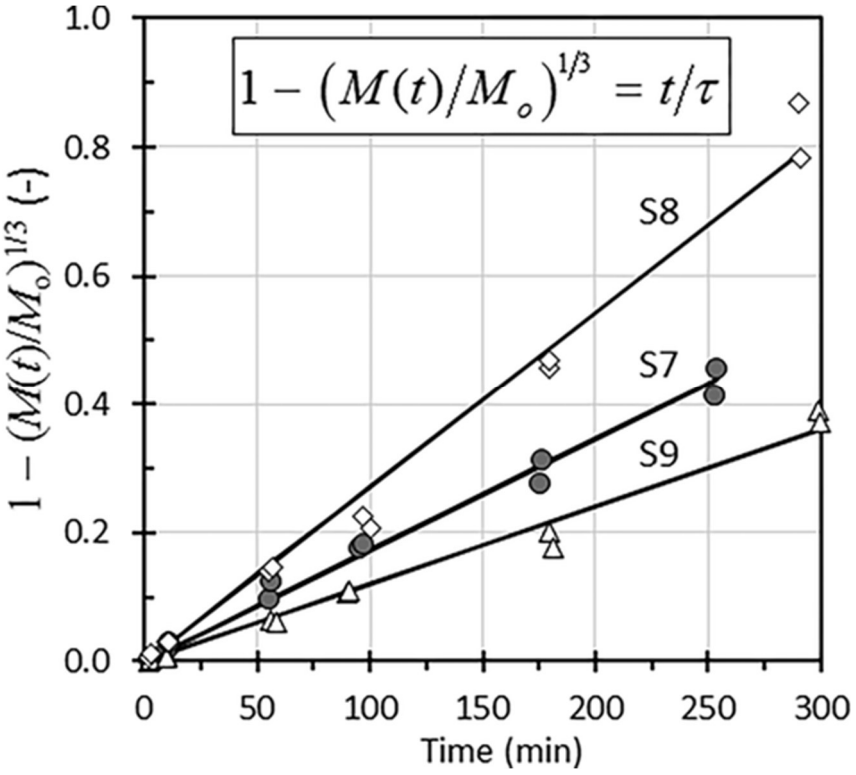

Figure 7. Dissolution curves obtained for selected TPS compounds plotted as indicated by eq 1.

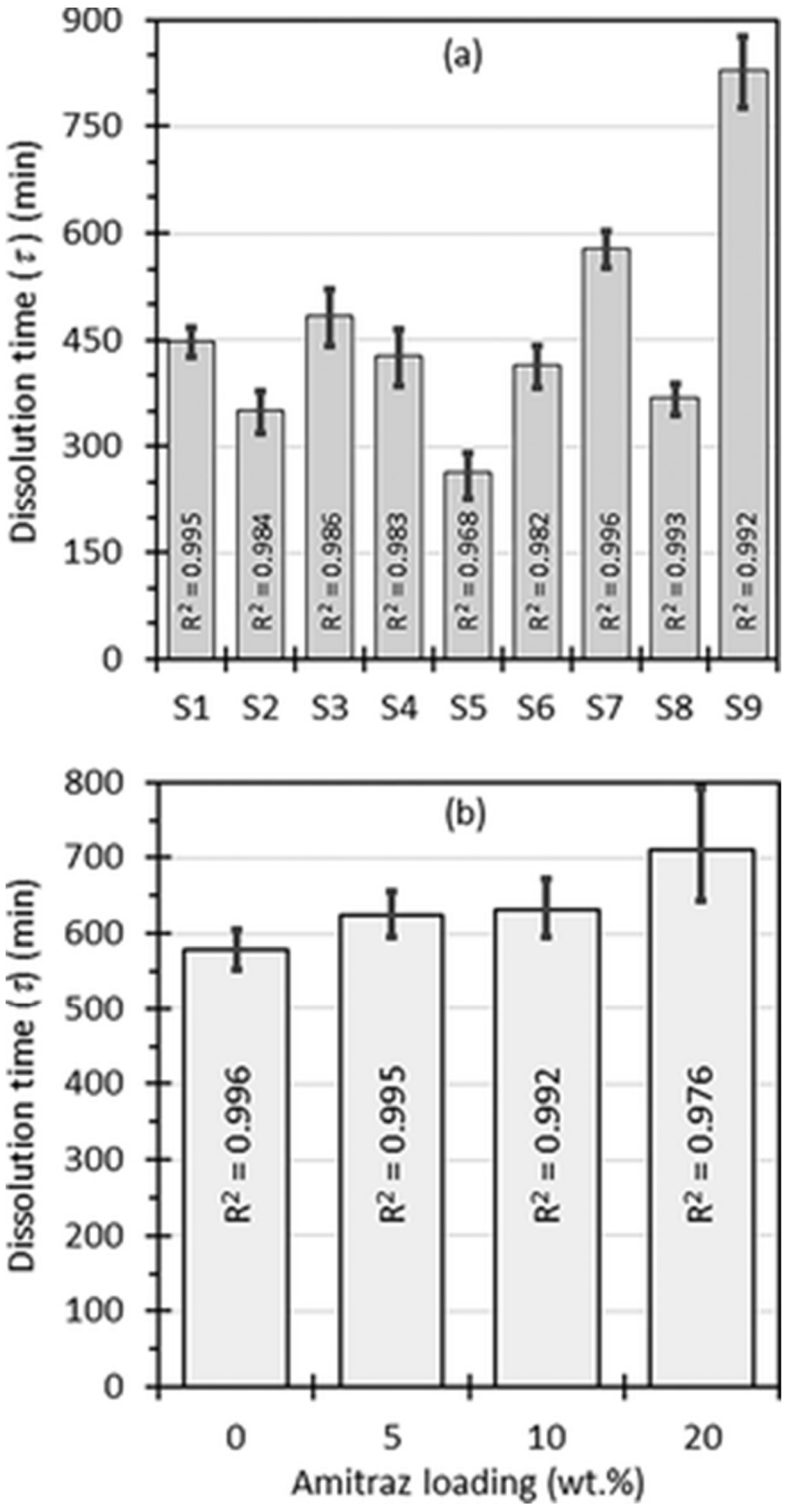

Figure 8. Experimental dissolution times (τ) for (a) the different dextrin nanocomposites, and (b) the effect of Amitraz loading level on the dissolution times (τ) with sample S7 serving as the carrier matrix. The error bars show the 95% confidence intervals for the dissolution time.

The composition corresponding to sample S7 was used as the carrier matrix for the acaricide. This selection was based on the relatively fast dissolution kinetics, limited retrogradation behavior and ease of extrusion of this compound. Figure 8b shows how the dissolution time varied with acaricide loading level. An upward trend toward longer

dissolution times is indicated, but the high variability of the measured values again means that the differences cannot be regarded as statistically significant at this stage. The only definitive conclusion that can be drawn from this data is that the Amitraz is fully released in water within about 12 h at the stirring conditions applied in the present dissolution experiments.

Figure 9 shows the particle size distributions measured in the liquid suspension formed after dispersion of the raw materials (Figure 9a) or complete dissolution of the compound granules (Figure 9b). The corresponding D5, D10 and D90 particle sizes are listed in Table 5. The neat Amitraz powder particles were the largest on average with a unimodal particle size distribution characterized by a long tail toward smaller particle sizes. The distributions for the dextrin and the dextrin TPS compounded in the complete absence of any additives (no glass beads included either) were bimodal. The compounding process, which converted the combination of dextrin, water, and glycerol into a thermoplastic material, did not materially change the D50 particle size observed in the dispersion. The implication is that the dextrin contains a cold-water-insoluble fraction that shows up in the PSD measurements. The CNF PSD was trimodal with a very wide range of particle sizes. It is possible, and likely, that the larger particles represent CNF agglomerates.

Table 5. Particle Sizes Measured after Dispersion of the Components in Water or Dissolution of Compound Granules in Water. The D5, D10 and D90 particle sizes are reported in µm

	neat components				**Amitraz content (wt %)**			
	CNF	**dextrin**	**Amitraz**	**S0[a]**	**0**	**5**	**10**	**20**
D5	12.1	6.78	80.6	2.87	4.24	4.18	4.05	3.11
D10	114	13.5	240	11.1	26.4	26.8	21.4	15.7
D90	725	20.7	510	24.2	336	224	311	109

[a]S0 is the additive free dextrin TPS compound described in Table 1.

Figure 9b shows the effect of Amitraz loading level on the particle size distribution in the final dispersions. All the PSD's are multimodal in nature with the different peaks probably associated with one or more of the constituents. The main peaks for sample A0 are approximately located at particle sizes corresponding to 15, 100, and 400 µm. The first represents, in the main, a contribution from the dextrin as this particle size is also observed in Figure 9a for both dextrin and sample S0. The two larger sizes are attributed to the CNF as they more or less agree with the CNF peaks in Figure 9a. As expected, these peaks all diminish in intensity, whereas the peak centered at ca. 15 µm grows in intensity as the Amitraz content of the compound increases. This means that most of the Amitraz particles released had that particular size. The implication is that formulating the Amitraz into a dextrin-based solid dosage form can facilitate the delivery of particles that are much smaller than the original Amitraz powder.

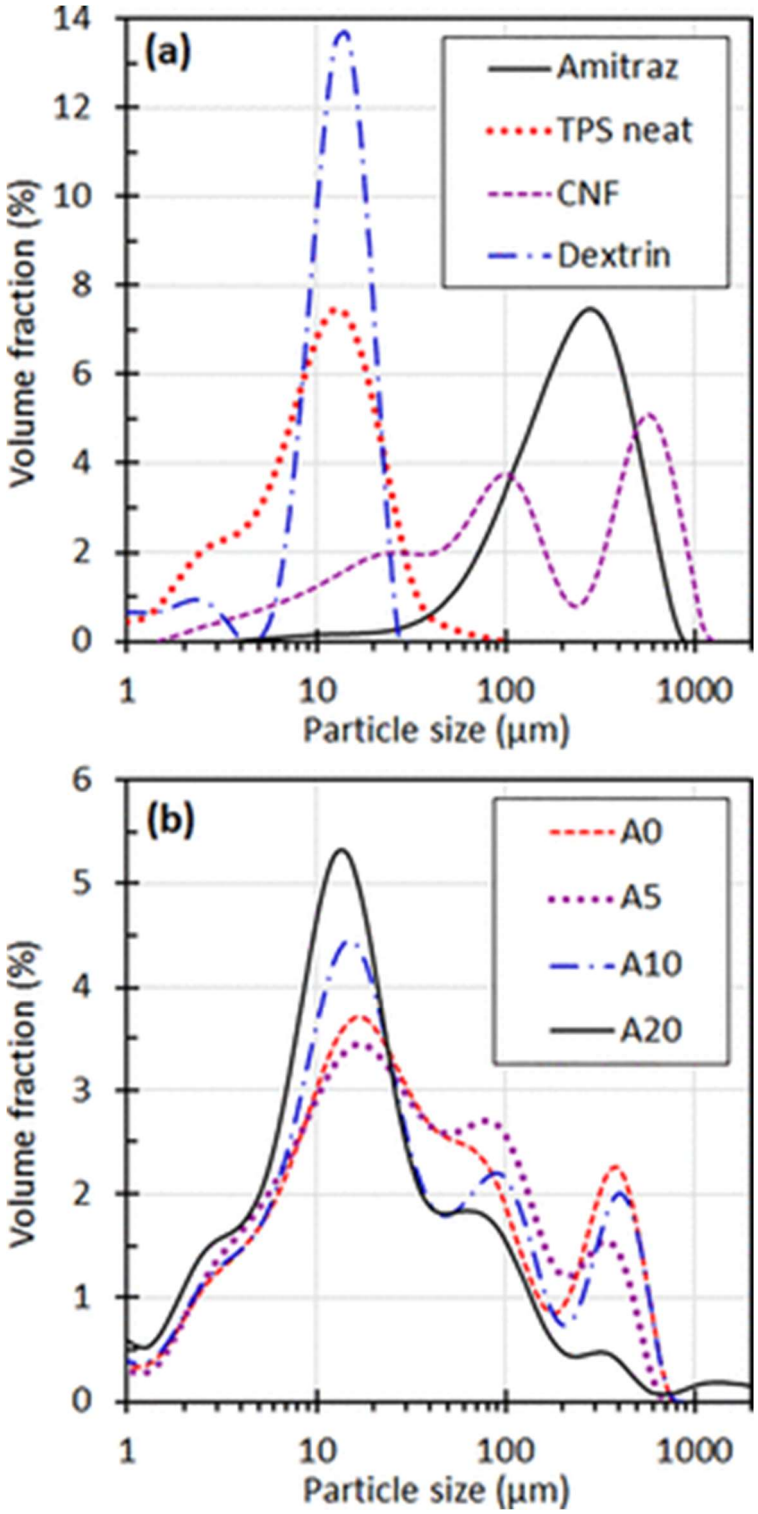

Figure 9. Particle size distribution observed in the suspensions formed on full dissolution of approximately 1 g of the granules in 500 mL of water of (a) raw materials and TPS without nanofillers and (b) compound materials with different Amitraz loadings.

Conclusions

Water-soluble dextrin-based thermoplastic starch nanocomposites were prepared by melt processing in a twin-screw compounder. These composites contained a 1:1 mixture of water and glycerol as plasticizer in addition to 4.0 wt % of selected additives or additive mixtures. The additives included cellulose nanofibers, stearic acid, and a layered double hydroxide clay. Cellulose nanofibers, included at 1.0 wt %, significantly improved the melt strength and surface smoothness of the extruded strand. The compounds all showed a beta transition close to −57 °C but the glass transition varied from 6 to 32 °C depending on the additives included in the formulation. XRD analysis revealed that all samples, except for the one containing only stearic acid as sole additive, suffered from retrogradation on aging for 98 days at room temperature and 75% relative humidity. The inclusion of the cellulose nanofibers at 1.0 wt % or LDH nanoclays at up to 4.0 wt % increased the bending modulus by about a factor of around three. The dissolution of the TPS granules in agitated water medium left only micrometer-sized biobased residues and followed Hixson–Crowell kinetics. The compound based on 1.0 wt % cellulose nanofibers and 3.00 wt % stearic acid was evaluated as the carrier matrix for Amitraz, a water insoluble acaricide. The dissolution time of ca. 5 mm granules was about 12 h, even at a 20 wt % active loading, and the acaricide was released in the form of very fine particles, with a D50 of about 15 µm.

Acknowledgments

Financial support for authors J.P. and H.O. from PAMSA and the Department of Science and Innovation under Grant DST/CON 0004/2019 is gratefully acknowledged. The authors also thank Jan Mentz and Greenfield Additives for kindly donating the hydrocalumite grade B44 sample, the layered double hydroxide (LDH) used in this study.

References

1. Collins, R.; Paul, Z.; Reynolds, D. B.; Short, R. F.; Wasuwanich, S. Controlled Diffusional Release of Dispersed Solute Drugs from Biodegradable Implants of Various Geometries. *Biomedical Sciences Instrumentation* **1997**, *33*, 137– 142
2. Schwartz, L.; Wolf, D.; Markus, A.; Wybraniec, S.; Wiesman, Z. Controlled-Release Systems for the Delivery of Cyromazine Into Water Surface. *J. Agric. Food Chem.* **2003**, *51* (20), 5972– 5976, DOI: 10.1021/jf034190j
3. Bell, G. A. The Structure/Physical Property Relationships of a Model Water-Dispersible Granule. *Pestic. Sci.* **1990**, *29* (4), 467– 473, DOI: 10.1002/ps.2780290410
4. Reddy, L. H.; Ghosh, B.; Rajneesh Fast Dissolving Drug Delivery Systems: A Review of the Literature. *Indian Journal of Pharmaceutical Sciences* **2002**, *64* (4), 331– 336
5. Yanagisawa, K.; Muroi, T.; Ohtsubo, T.; Watano, S. Effect of Binder Composition on Physicochemical Properties of Water Dispersible Granules Obtained Through Direct Granulation of Agrochemical Suspension Using Fluidized Bed. *J. Pestic. Sci.* **2017**, *42* (3), 112– 115, DOI: 10.1584/jpestics.D17-017
6. Sandell, L. S.; Wysong, R. D. Water-dispersible Granular Agricultural Compositions Made By Heat Extrusion. U.S. 5 714 157, 1998.

7. Bahrainian, S.; Abbaspour, M.; Kouchak, M.; Taghavi Moghadam, P. A. Review on Fast Dissolving Systems: From Tablets to Nanofibers. *Jundishapur Journal of Natural and Pharmaceutical Products* **2016**, *12* (2), e34267, DOI: 10.5812/jjnpp.34267
8. van Soest, J. J. G.; Hulleman, S. H. D.; de Wit, D.; Vliegenthart, J. F. G. Crystallinity in Starch Bioplastics. *Ind. Crops Prod.* **1996**, *5* (1), 11– 22, DOI: 10.1016/0926-6690(95)00048-8
9. Fu, Z.; Chen, J.; Luo, S.-J.; Liu, C.-M.; Liu, W. Effect of Food Additives on Starch Retrogradation: A Review. *Starch - Stärke* **2015**, *67* (1–2), 69– 78, DOI: 10.1002/star.201300278
10. Kvien, I.; Sugiyama, J.; Votrubec, M.; Oksman, K. Characterization of Starch Based Nanocomposites. *J. Mater. Sci.* **2007**, *42* (19), 8163– 8171, DOI: 10.1007/s10853-007-1699-2
11. Jiménez, A.; Fabra, M. J.; Talens, P.; Chiralt, A. Phase Transitions in Starch Based Films Containing Fatty Acids. Effect On Water Sorption and Mechanical Behaviour. *Food Hydrocolloids* **2013**, *30* (1), 408– 418, DOI: 10.1016/j.foodhyd.2012.07.007
12. Lendvai, L.; Sajó, I.; Karger-Kocsis, J. Effect of Storage Time on the Structure and Mechanical Properties of Starch/Bentonite Nanocomposites. *Starch - Stärke* **2019**, *71* (1–2), 1800123, DOI: 10.1002/star.201800123
13. Wang, S.; Li, C.; Copeland, L.; Niu, Q.; Wang, S. Starch Retrogradation: A Comprehensive Review. *Compr. Rev. Food Sci. Food Saf.* **2015**, *14* (5), 568– 585, DOI: 10.1111/1541-4337.12143
14. Battegazzore, D.; Bocchini, S.; Nicola, G.; Martini, E.; Frache, A. Isosorbide, a Green Plasticizer for Thermoplastic Starch That Does Not Retrogradate. *Carbohydr. Polym.* **2015**, *119*, 78– 84, DOI: 10.1016/j.carbpol.2014.11.030
15. Area, M. R.; Rico, M.; Montero, B.; Barral, L.; Bouza, R.; Lopez, J.; Ramirez, C. Corn Starch Plasticized with Isosorbide and Filled with Microcrystalline Cellulose: Processing and Characterization. *Carbohydr. Polym.* **2019**, *206*, 726– 733, DOI: 10.1016/j.carbpol.2018.11.055
16. Jiménez, A.; Fabra, M. J.; Talens, P.; Chiralt, A. Effect of Re-crystallization on Tensile, Optical and Water Vapour Barrier Properties of Corn Starch Films Containing Fatty Acids. *Food Hydrocolloids* **2012**, *26* (1), 302– 310, DOI: 10.1016/j.foodhyd.2011.06.009
17. Ojijo, V.; Sinha Ray, S. Processing Strategies in Bionanocomposites. *Prog. Polym. Sci.* **2013**, *38* (10–11), 1543– 1589, DOI: 10.1016/j.progpolymsci.2013.05.011
18. Dufresne, A.; Dupeyre, D.; Vignon, M. R. Cellulose Microfibrils from Potato Tuber Cells: Processing and Characterization of Starch–Cellulose Microfibril Composites. *J. Appl. Polym. Sci.* **2000**, *76* (14), 2080– 2092, DOI: 10.1002/(SICI)1097-4628(20000628)76:14<2080::AID-APP12>3.0.CO;2-U
19. Ferreira, F. V.; Dufresne, A.; Pinheiro, I. F.; Souza, D. H. S.; Gouveia, R. F.; Mei, L. H. I.; Lona, L. M. F. How Do Cellulose Nanocrystals Affect the Overall Properties of Biodegradable Polymer Nanocomposites: A Comprehensive Review. *Eur. Polym. J.* **2018**, *108*, 274– 285, DOI: 10.1016/j.eurpolymj.2018.08.045
20. Sun, J.; Zhao, R.; Zeng, J.; Li, G.; Li, X. Characterization of Destrins With Different Dextrose Equivalents. *Molecules* **2010**, *15* (8), 5162– 5173, DOI: 10.3390/molecules15085162

21. Mohammadi Nafchi, A.; Moradpour, M.; Saeidi, M.; Alias, A. K. Thermoplastic Starches: Properties, Challenges, and Prospects. *Starch-Stärke* **2013**, *65* (1–2), 61–72, DOI: 10.1002/star.201200201
22. Labuschagné, J.; Molefe, D.; Focke, W. W.; Ofosu, O. Layered Double Hydroxide Derivatives as Flame Retardants for Flexible PVC. *Macromol. Symp.* **2019**, *384* (1), 1800148, DOI: 10.1002/masy.201800148
23. Greenspan, L. Humidity Fixed Points of Binary Saturated Aqueous Solutions. *J. Res. Natl. Bur. Stand., Sect. A* **1977**, *81* (1), 89– 96, DOI: 10.6028/jres.081A.011
24. Frost, K.; Kaminski, D.; Kirwan, G.; Lascaris, E.; Shanks, R. Crystallinity and Structure of Starch Using Wide Angle X-Ray Scattering. *Carbohydr. Polym.* **2009**, *78* (3), 543–548, DOI: 10.1016/j.carbpol.2009.05.018
25. Vähäsalo, L.; Holmbom, B. Reliable Spectrophotometric Determination of Starch Concentration in Papermaking Process Waters. *Nord. Pulp Pap. Res. J.* **2004**, *19* (1), 75– 77, DOI: 10.3183/npprj-2004-19-01-p075-077
26. Hixson, A. W.; Crowell, J. H. Dependence of Reaction Velocity Upon Aurface and Agitation: I—Theoretical Consideration. *Ind. Eng. Chem.* **1931**, *23* (8), 923–931, DOI: 10.1021/ie50260a018
27. De Blaey, C.; Van der Graaff, H. Dissolution Kinetics of Soluble Nondisintegrating Disks. *J. Pharm. Sci.* **1977**, *66* (12), 1696– 1699, DOI: 10.1002/jps.2600661210
28. Liu, H.; Xie, F.; Yu, L.; Chen, L.; Li, L. Thermal Processing of Starch-Based Polymers. *Prog. Polym. Sci.* **2009**, *34* (12), 1348– 1368, DOI: 10.1016/j.progpolymsci.2009.07.001
29. Obiro, W. C.; Sinha Ray, S.; Emmambux, M. N. V-amylose Structural Characteristics, Methods of Preparation, Significance, and Potential Applications. *Food Rev. Int.* **2012**, *28* (4), 412– 438, DOI: 10.1080/87559129.2012.660718
30. Castaño, J.; Rodríguez-Llamazares, S.; Contreras, K.; Carrasco, C.; Pozo, C.; Bouza, R.; Franco, C. M. L.; Giraldo, D. Horse Chestnut (Aesculus hippocastanum L.) Starch: Basic Physico-chemical Characteristics and Use As Thermoplastic Material. *Carbohydr. Polym.* **2014**, *112*, 677– 685, DOI: 10.1016/j.carbpol.2014.06.046
31. Nindiyasari, F.; Griesshaber, E.; Zimmermann, T.; Manian, A. P.; Randow, C.; Zehbe, R.; Fernandez-Diaz, L.; Ziegler, A.; Fleck, C.; Schmahl, W. W. Characterization and Mechanical Properties Investigation of the Cellulose/Gypsum Composite. *J. Compos. Mater.* **2016**, *50* (5), 657– 672, DOI: 10.1177/0021998315580826